Progress In Electromagnetics Research B, Vol. 18, 25–42, 2009

THE NOVEL TWO PHASE FIELD-ASSISTED HYBRID SRG: MAGNETIO STATIC FIELD ANALYSIS, SIMULATION, AND EXPERIMENTAL CONFIRMATION

E. Afjei and H. Torkaman

Department of Electrical Engineering
Shahid Beheshti University, G.C.
Tehran, Iran

Abstract—This paper introduces a new configuration for a two phase field assisted hybrid switched reluctance generator, which can operate in motoring mode as well. This concept allows higher output power production compare to standard SRG. The proposed novel generator consists of two magnetically independent stator and rotor sets (layers), where each stator set includes four salient poles with windings wrapped around them, while the rotor comprises of two salient poles with different arc lengths and no windings. There is a stationary reel, which has the field coils wrapped around it and is placed between the two-stator sets. In this format, the developed magnetic field from the stator poles travels to the rotor then to the rotor shaft and finally completes its path via the generator housing. To evaluate the generator performance, two types of analysis, namely the numerical technique and the experimental study have been utilized. The analysis is carried out for the machine in self exited generator mode as well as field assisted mode. In the numerical analysis, the finite element analysis is employed, whereas in the experimental study, a proto-type generator has been built and tested.

1. INTRODUCTION

Variable speed brushless motors as well as generators are gaining considerable attention for different high performance applications requiring low cost and maintenance. The switched reluctance motor/generator is one of the challengers for low cost and simple structure in variable speed drive applications such as hybrid cars, home appliances, and wind turbines.

Corresponding author: E. Afjei (E-Afjei@sbu.ac.ir).

Switched Reluctance Generator (SRG) is an attractive solution for worldwide increasing demand of electrical energy [1]. The SRG has various desirable features namely, simple and solid structure, easiness of maintenance, small moment of rotor inertia, support of both high-rotational speed and high-temperature operation, and low manufacturing cost because the SR generator has no rotor windings and no permanent magnet [2–4]. Advantages of using SRG have been proved for some applications like starter/generator for gas turbine [5–7], wind turbine generator [8–11], battery charger [12], flux-compression electromechanical converter [13], and as an alternator for automotive applications [14–16]. The aerospace and automotive applications are generally characterized by high-speed operation. The wind energy application is characterized by low-speed high-torque operation [1].

The combination of switched reluctance motor with a field assisted generator looks a very promising arrangement for variable speed applications. In the previous work [17, 18] a new hybrid reluctance motor/field-assisted generator has been proposed. In there, the ability and the potentially of this unit for being used in hybrid vehicle has been mentioned.

Due to the rising demand for higher power and reduction of fuel consumption in cars, the concept of starter-generator has been investigated over the past several years. The application of electrical machines and drives systems in all-electric and hybrid-electric vehicles has been widely reported in recent years [19–22].

This paper presents a new configuration for a two phase unidirectional SR motor/field assisted generator which is organized as follows; Section two explains the motor/generator construction, section three contains the numerical analysis of the prototype machine and section four includes the physical assembly of the machine as well as the experimental results obtained from the new hybrid switched reluctance motor/generator followed by conclusions in section five.

2. MOTOR/GENERATOR DESCRIPTION

The proposed novel motor/generator consists of two magnetically independent stator and rotor sets (layers), where each stator set includes four salient poles having 45° arc length with coils wrapped around them, while the rotor comprises of two salient poles with different arc lengths and no windings. The rotor is shaped in such a way to produce starting torque as well as having rising inductance in all of 90° rotor arc length. The arc of each rotor pole is the same as stator pole (45°) in one side and twice as much in the other side.

The shape of rotor in each side is shown in Fig. 1(a), the actual rotor assembly is shown in Fig. 1(b), and finally, the stator laminations is shown in Fig. 1(c).

The two layers are exactly symmetrical with respect to a plane perpendicular to the middle of the motor shaft. Since this assembly is a two phase motor/generator; therefore, each layer consists of four stator poles and two rotor poles, respectively. In the motoring operation each layer operates independently, but in exact sequence with each other. In other words, each layer consist of a four by two reluctance motor configuration sharing common shaft which operating in sequence. There is a stationary reel, which has the field coils wrapped around it and is placed between the two-stator sets. This reel has a rotating cylindrical core, which guides the magnetic field. The magnetic flux produced by the coils travels through the guide and shaft to the rotor and then to the stator poles, and finally closes itself through the motor housing. Therefore, in the generator mode, one set of rotor poles is

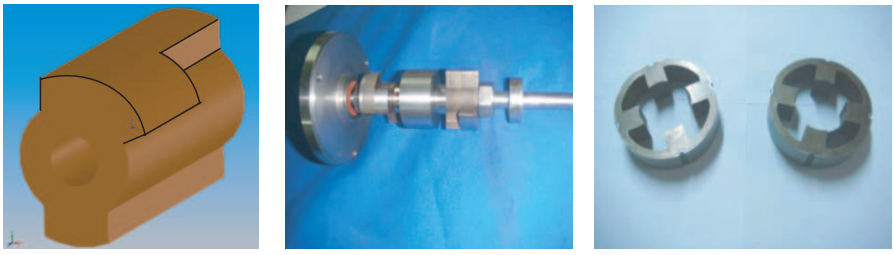

(a) (b) (c)

Figure 1. (a) Rotor shape. (b) Actual rotor assembly. (c) Stator laminations.

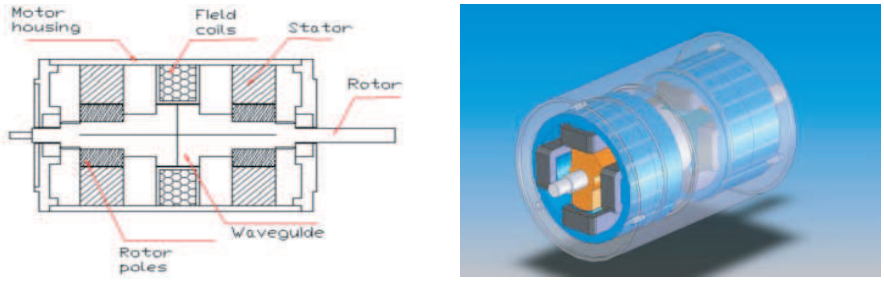

(a) (b)

Figure 2. (a) A cut view of the motor/generator. (b) The complete motor/generator assembly.

magnetically north while the other set is magnetically south. In this machine, the magnetic field has been induced to the rotor without using any brushes. A cut view of the motor/generator is shown in Fig. 2(a).

In order to get a better view of the motor/generator configuration, the complete motor/generator assembly is shown in Fig. 2(b).

There are two stators and rotors sections placed on both sides of the field coil assembly which has the rotor shaft as its main core and two front/end caps plus the motor housing. A set of photo interrupters are also placed in the back of the motor for the detection of rotor position. Two types of analysis, namely numerical and experimental have been performed.

3. NUMERICAL ANALYSIS

The design of the motor/generator becomes complicated due to complex geometry and material saturation. The reluctance variation of the generator has an important role on the performance; hence an accurate knowledge of the flux distribution inside the generator for different excitation currents and rotor positions is essential for the prediction of generator performance. The generator can be highly saturated under normal operating conditions. To evaluate properly the motor/generator design and performance a reliable model is required. The finite-element technique can be conveniently used to obtain the magnetic vector potential values throughout the generator in the presence of complex magnetic circuit geometry and nonlinear properties of the magnetic materials. These vector potential values can be processed to obtain the field distribution, torque, and flux linkage.

The 3-D field analysis has been performed using a MagNet CAD package [23]. This analysis is based on the variational energy minimization technique to solve for the magnetic vector potential. The partial differential equation for the magnetic vector potential is given by [24–26];

$$-\frac{\partial}{\partial x}\left(\gamma\frac{\partial \bar{A}}{\partial x}\right)-\frac{\partial}{\partial y}\left(\gamma\frac{\partial \bar{A}}{\partial y}\right)-\frac{\partial}{\partial z}\left(\gamma\frac{\partial \bar{A}}{\partial z}\right)=J \tag{1}$$

where, A is the magnetic vector potential. In the variational method the solution to Equation (1) obtained by minimizing the following functional [24–26];

$$F(A)=\frac{1}{2}\iiint_{\Omega}\left[\gamma\left(\frac{\partial A}{\partial x}\right)^2+\gamma\left(\frac{\partial A}{\partial y}\right)^2+\gamma\left(\frac{\partial A}{\partial z}\right)^2\right]d\Omega-\iiint_{\Omega}JAd\Omega \tag{2}$$

Table 1. SR M/G dimensions.

Parameter	Value
Stator core outer diameter	72 mm
Stator core inner diameter	62 mm
Stator arc	45 deg
Air gap	0.25 mm
Rotor core outer diameter	39.5 mm
Rotor shaft diameter	10 mm
Rotor larger arc	90 deg
Rotor smaller arc	45 deg
Stack length	35 mm
Number of turns per pole	120
Number of turns for field coil	400

where, Ω is the problem region of integration. In the three dimensional finite element analysis tetrahedral elements with dense meshes at places where the variation of fields are greater have been used. The generator specifications considered for the study are depicted in Table 1.

The analysis is carried out for the machine in two different modes of operation, namely self exited and field assisted modes. In the self exited mode of operation, the proper stator coils in each layer have been switched on while the field coil is turned off. Due to unsymmetrical rotor structure, two different directions of rotation are considered in the self exited mode. In this mode there is no field current in the center coil and power generation is carried out by energizing the proper stator coils during the negative inductance periods.

3.1. Self Exited Generator Mode

When the machine is driven by a prime mover and stator windings are excited during the negative slope of the phase inductance then generating torque can be produced.

The torque in a SRG can be expressed in unsaturated conditions as;

$$T = \frac{1}{2}\frac{dL}{d\theta}i^2 \tag{3}$$

where, L is the phase inductance, and θ is the rotor position angle.

This equation means that the torque is negative in the region of $dL/d\theta < 0$. When the stator windings are excited in that region and

the rotor is driven by a proper prime mover, the mechanical energy can be transformed into electric energy. In other words, generation torque is produced when the phase winding is energized during the negative slope of the phase inductance variation, (i.e., after complete rotor/stator poles alignment).

The motor/generator with and without the housing used in the numerical analysis are shown in Figs. 3(a), (b), and (c). The 3-D

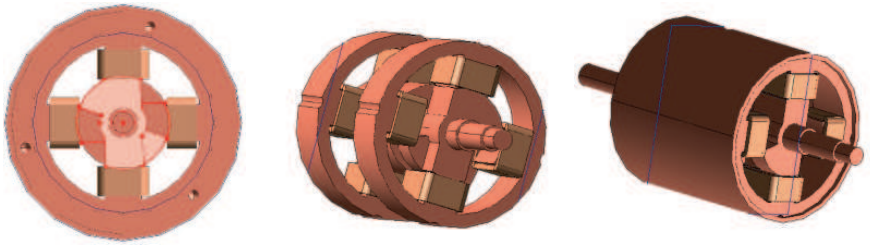

(a) (b) (c)

Figure 3. Model of SR generator. (a) Front view. (b) Without housing. (c) With housing.

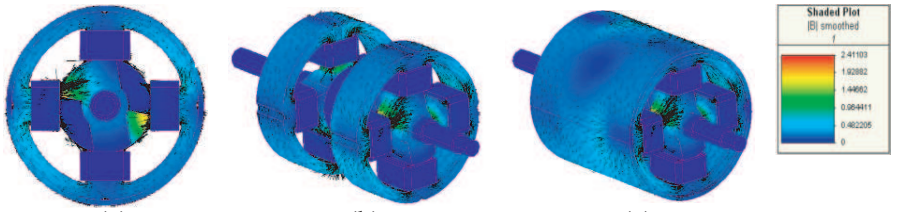

(a) (b) (c)

Figure 4. 3-D magnetic field densities for start of alignment case in self excited mode.

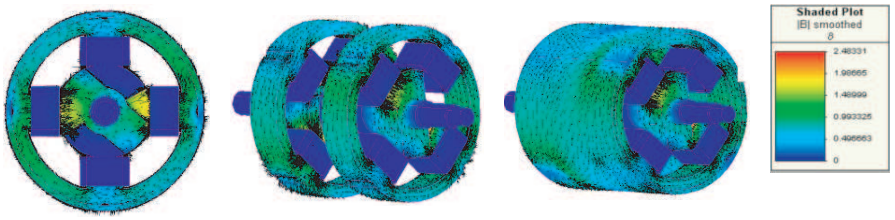

(a) (b) (c)

Figure 5. 3-D magnetic field densities for half-aligned case in self excited mode.

field analysis has been performed using a commercial finite element package [23], which is based on the variational energy minimization technique to solve for the magnetic vector potential. The stator and rotor cores are made up of M-27 non-oriented silicon steel laminations [23].

Figures 4(a), (b), and (c) show the magnetic flux density for non-aligned when the machine operates as a self exited generator and each layer is operating independently.

Figures 5(a), (b), and (c) show the magnetic flux density for half aligned case when the machine operates as a self exited generator and each layer is operating independently. Figs. 6(a), (b), and (c) show the magnetic flux density for fully aligned case when the machine operates as a self exited generator and each layer is operating independently

The magnitude of magnetic flux density in the stator poles with energized coil starts from 0.5 Tesla at the beginning of rotor/ stator pole alignment shown in Fig. 4(a) and increases to 1.2 Tesla for half alignment shown in Fig. 5(a) and then reaches to 1.45 Tesla at full alignment in Fig. 6(a). The same type of behavior for magnetic flux density can be seen in the generator yoke. The direction of magnetic

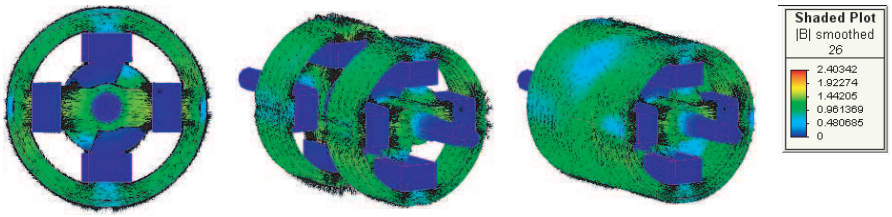

Figure 6. 3-D magnetic flux densities for fully aligned case in self excited mode.

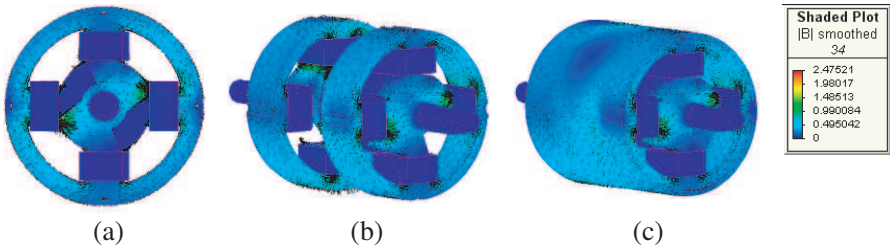

Figure 7. 3-D magnetic flux densities for end of alignment case in self excited mode.

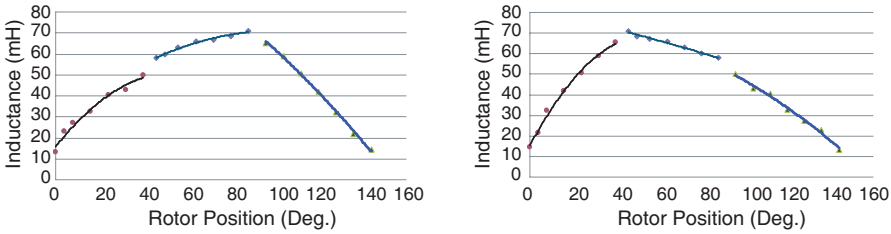

Figure 8. Terminal inductance vs. rotor position for (a) CCW direction, (b) CW direction.

flux travels from one energized stator pole winding to the yoke and then to the opposite stator pole as shown in Fig. 4(b)–Fig. 7(b). The flux pattern shaped over the motor housing shown in Fig. 4(c)–Fig. 7(c) indicates some of the magnetic field produced in the front layer travels through the motor housing to the back layer even though these two layers are operating independently.

The inductance has been defined as the ratio of each phase flux linkages to the exciting current (λ/I). Values based on this definition are presented for counter clock wise (CCW) and clock wise (CW) directions in Fig. 8(a), and Fig. 8(b) respectively, for current of 3 A.

In the Fig. 8, zero degree is considered to be as the unaligned case. The inductance profile shows steady increase as the rotor poles move into alignment with the stator poles, hence positive torque can be obtained from 0° to 90° of rotor arc. The inductance versus rotor position data has been depicted by three curves one from 0° to 45° (first rotor step), the second one from 45° to 90° (second rotor step) and finally the third one from 90° to 145°. The generating interval for CCW rotation is twice as much as the one in the CW rotation. The generated voltage can be obtained from the phase inductance versus rotor position by;

$$e_{ind} = \frac{\partial \lambda}{\partial t} = \frac{\partial (Li)}{\partial t} = L\frac{\partial i}{\partial t} + i\frac{\partial L}{\partial t} \tag{4}$$

Since current, i is kept constant and $(\partial\theta/\partial t) = \omega$ then Equation (4) can be rewritten as:

$$e_{ind} = i\frac{\partial L}{\partial \theta}\omega = N\frac{\partial \phi}{\partial \theta}\omega \tag{5}$$

where, ω is motor angular speed in rad/sec.

The shape of generated voltage during negative slope of phase inductance is obtained in clock wise (CW) as well as CCW direction

by the inductance profile shown in Fig. 9 and Equation (5) for a speed of 1000 rpm.

Due to the negative slope of the phase inductance, the magnitude of generated voltage is negative. As a result of unsymmetrical rotor shape, the generating period in CCW direction is twice as much as in CW direction.

At this point the field coil is energized and second mode of operation begins.

3.2. Field Assisted Mode

In the field assisted generator mode of operation, the field coil between the two-stator sets is at 0.25 A. Fig. 10(a) shows the direction of the

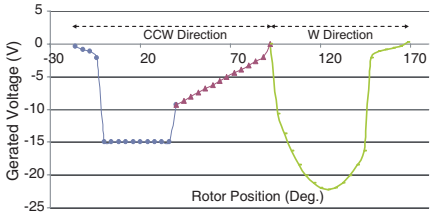

Figure 9. Generated voltage vs. rotor position.

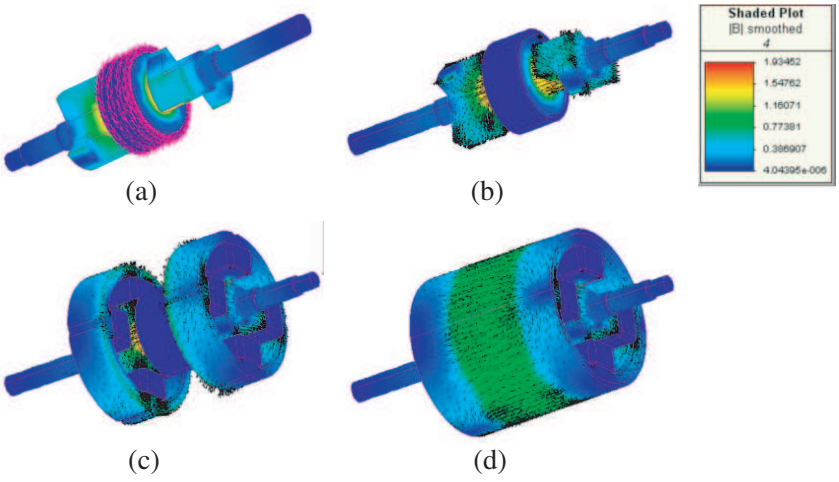

Figure 10. The current density, magnetic flux density and flux direction in field assisted mode in: (a) The field coil and shaft. (b) The rotor poles. (c) Rotor/stator assembly. (d) The generator housing.

current in the center field coil as well as the magnetic flux density and Figs. 10(b), (c), and (d) show the magnetic flux density as well as the flux direction in the generator shaft, the rotor poles, rotor and stator assembly, and the generator housing, respectively.

In Fig. 10(a), the magnetic field produced by the coil travels through the shaft to the rotor poles and high magnetic flux densities has been produced under the rotor poles. The rotor poles in front and back have magnetically North and South Pole configurations, respectively.

Figure 10(b) shows the field coming out of the rotor pole tips perpendicularly and going into the respected stator poles. Finally, the magnetic flux pattern is shaped over the generator housing in which the flux travels from one set to the other set as is shown in Fig. 10(d).

The flux linkage versus rotor position obtained by simulation for one of the stator pole windings is shown in Fig. 11.

In order to estimate the shape of generated voltage, the flux linkage data points have been divided into five different segments. The different parts of flux linkage curve can be explained in the following fashion. The first part is the segment before stator/rotor pole alignment, the second part starts at the beginning of stator/rotor pole alignment up to half aligned case, the third part is from half aligned to full aligned case, the fourth region begins at the start of unaligned rotor/ stator pole up half unaligned case, and finally all the way to unaligned position.

A third order equation has been fitted through the data points for each part of the flux linkage curve. The equations are presented in Table 2.

The shape of induced voltage for a speed of 1000 rpm, using the different flux linkage curves obtained above and Equation (5) is shown in Fig. 12.

As seen from Fig. 12, the maximum generated voltage has occurred at half aligned case. The generated voltage in Fig. 12 has different

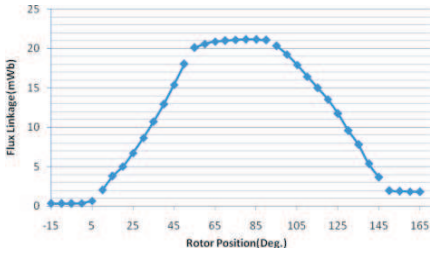

Figure 11. The flux linkage.

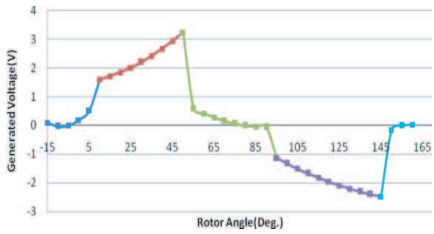

Figure 12. Generated voltage.

Table 2. Function coefficients.

$F(\theta)$	θ (Deg)
$0.00018\theta^3 + 0.00459\theta^2 + 0.03136\theta + 0.38$	$[-15, 5]$
$0.000031\theta^3 + 0.00072\theta^2 + 0.2567\theta - 0.54$	$[5, 50]$
$0.000031\theta^3 - 0.00844\theta^2 + 0.7482\theta - 0.7$	$[50, 90]$
$0.000014\theta^3 - 0.00762\theta^2 + 0.8512\theta - 4.33$	$[90, 145]$
$-0.00013\theta^3 + 0.0636\theta^2 - 10.11\theta - 492.2$	$[145, 165]$

distinct parts which can be explained in the following manner. The first part $[-15^\circ,\ 5^\circ]$ is when the rotor pole moves closer to the stator pole and the generated voltage tends to increase. In the second segment $[5^\circ,\ 50^\circ]$, the rotor pole starts overlapping the stator pole. The phase inductance at this rotor position jumps to a higher value and begins increasing as the rotor pole aligns itself with stator pole. Since the phase current is considered to be constant in the simulation therefore, the generated voltage rises as the phase inductance increases. Finally, it reaches its maximum value at half alignment. It is worth mentioning that, at this rotor position, the pole belonging to the next phase state its alignment therefore, some of the magnetic flux is directed to this phase and the magnetic flux density reduces in the first phase. In the third section $[50^\circ,\ 90^\circ]$, the first rotor pole is in half aligned position and going to full alignment and the second rotor pole moving into half aligned position, therefore the generated voltage drops due to the magnetic flux density reduction in that phase. Finally, in the fourth part $[90^\circ,\ 145^\circ]$, the rotor pole is going into unaligned position and negative voltage is generated due to the negative slope of the flux linkage curve. The estimated average voltage is about 1 volt for the voltage curve shown in Fig. 12.

At this point it is imperative to look at the field coil inductance curve to see how it varies as the rotor turns because it can provide useful information in order to explain the difference in the simulated voltage curve with the experimental one. Fig. 13 shows the calculated field inductance versus rotor position obtained by the ratio of flux linkage to the field current.

The maximum inductance occurs at every 45° since the field coil perceives two rotor pole sets which are positioned perpendicular to each other. When one rotor pole set is in full unaligned position with the stator poles the other rotor pole set is in full alignment with the other stator poles. In the above simulation, field current considered to be constant but in actual circuit the field voltage is constant and current will have some variation due to the changes in inductance value.

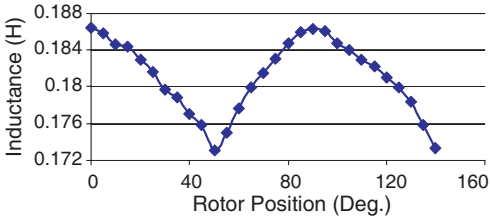

Figure 13. The calculated field inductance vs. rotor position.

(a) (b)

Figure 14. (a) Different motor/generator parts. (b) The actual motor/generator.

4. EXPERIMENTAL RESULTS

The generator has been fabricated and tested for performance and functionality in the laboratory. Fig. 14(a) illustrates the different parts of the novel motor/generator before being assembled in the laboratory while Fig. 14(b) shows the complete motor/generator. In the housing of the motor/generator assembly four grooves have been cut out and filled with motor laminations in order to reduce the reluctance of the housing in such a way that the magnetic flux is able to travel through the motor housing much easier.

In order to synchronize the proper firing of phase windings with the rotor position a discrete shaft sensor is installed in the back of the generator. The sensor is composed of two opto-couplers, one for each layer and a slotted disc with two 90° openings for the CCW direction and 45° openings for CW direction. Fig. 15 shows a set of opt-couplers with slotted disc as shaft position sensor is installed on the back of the generator in order to synchronize the proper firing of each phase transistor for CCW.

There are four 90° pulses produced by the motor shaft position sensors in each rotation. When one signal is in its high state the other one is in its low state. Each pulse appears 2 times in one rotation for each phase since this is a two phase generator.

In the field assisted mode, the shaft of the generator is connected to a motor to act as a prime mover. The speed of the motor is kept constant for various field currents; the resulting terminal voltage for only one pole winding after being rectified is shown in Fig. 17.

In these figures curve fitting (power) has been used for better presentation of the data points.

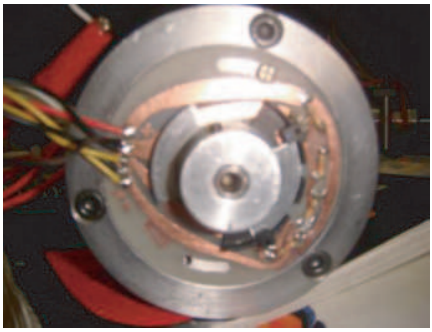

Figure 15. Direct shaft position sensors.

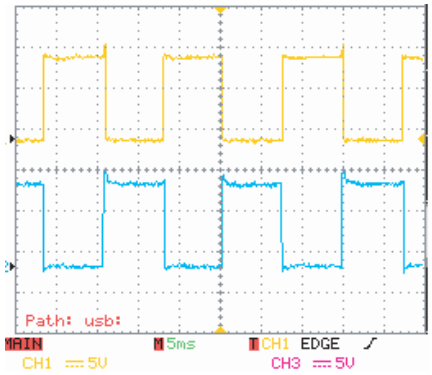

Figure 16. The output signals from the photo-interrupters.

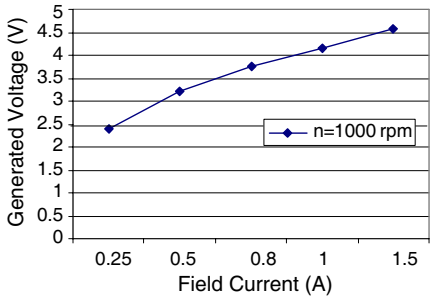

Figure 17. Generator terminal voltage vs. field current.

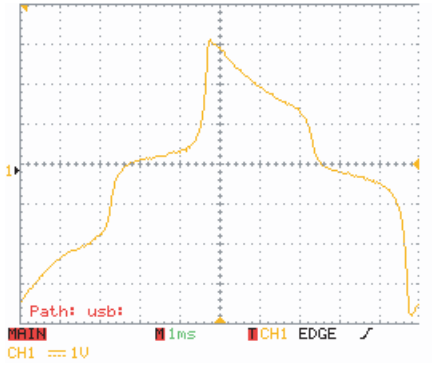

Figure 18. The actual output voltage for one of the stator pole winding at no load (field assisted mode).

The minimum voltage is about 2.4 volt at a field current of 0.25 A at 1000 rpm, which is within close agreement (less than 20%) with the computed average voltage resulted by simulation. One of the reasons for the production of the error is considering the field current to be constant in the simulation while it actually fluctuates in real generator unit.

The actual output voltage for one of the stator pole winding at no load for field assisted mode of operation is also shown in Fig. 18.

Due to the shape of the stator and rotor poles and saturation inside them, the generated output voltage has harmonics which is typical in this type of motor/generator unit.

The shape of this voltage waveform has some differences with the voltage waveform found numerically (Fig. 12). One of the main reasons for this discrepancy is because of the current variation due to the changes in the field inductance values which, has not been not considered in the simulation. In order to be able to explain the shape of the generated voltage, the field current and one of the phase output voltage are shown together in Figs. 19(a) and (b), respectively.

As the rotor turns the field current fluctuates around a dc value. This variation is due to the changes in the phase inductance value which in turn, affects the shape of output voltage.

When the rotor poles reach the stator poles, the output voltage rises to a maximum value (Fig. 19(b)), and then starts decreasing as the rotor poles go into more alignment with stator poles, at the same time, the field current begins to descend due to production of high phase inductance value caused by stator/rotor poles alignment.

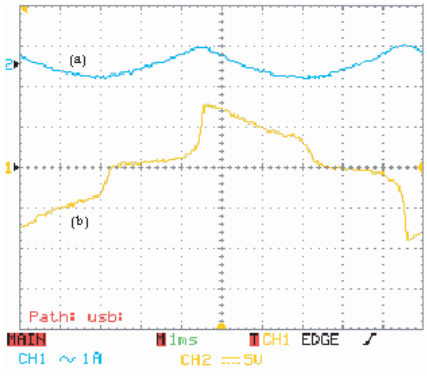

Figure 19. Current and voltage waveforms (field assisted mode) (a) Field current, (b) Output voltage.

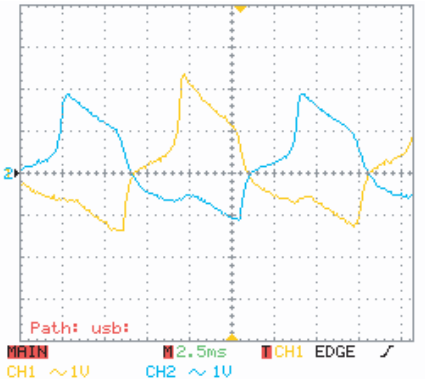

Figure 20. The actual current for two stator pole windings CW rotation (self excited mode).

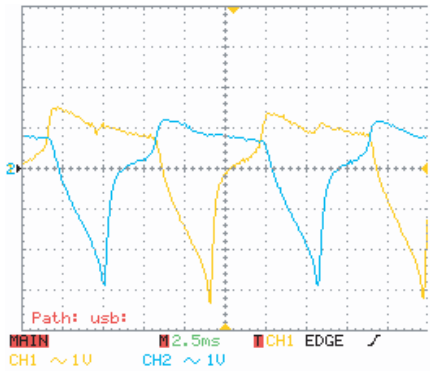

Figure 21. The actual current for two stator pole windings CCW rotation (self excited mode).

The generator in the self excited mode of operation is connected to a prime mover and a two switched per phase drive circuit. The speed of rotation is set at 1000 rpm. The actual output currents going in and out of machine for two stator pole windings in CW rotation is shown in Fig. 20.

The first part of the waveform has positive current magnitude which means the power is leaving the machine (generating mode) while the negative magnitude of the waveform denotes the current entering the unit (motoring mode). As seen from Fig. 20, there is always positive current exists during a full rotation which denotes continuous current production in each rotation. In CW rotation, the positive and negative parts of the current waveform have exactly the same generating periods. Fig. 21 shows the actual current for two stator pole windings in CCW rotation.

The unit works as a generator in the positive part of the current waveform and as a motor in the negative part of current waveform. Due to the unsymmetrical shape of rotor, the generating period is twice as long as motoring part. There is always a positive current magnitude during a full rotation which denotes a continuous current production for each full rotation.

Due to new rotor geometry which comprises of two salient poles with different arc lengths, this SRG can produces output voltage in 360 degrees of rotor rotation. As calculated from the result of generated voltage from field assisted mode of operation the efficiency of the machine with its converter increased by 29%. In other words, these results confirmed that the choice of new topology of the SRG has demonstrated that the SR generator exhibited higher performance in

terms of efficiency under loads. This feature plays important rule in power production in wind turbine or in hybrid vehicle.

5. CONCLUSION

In this paper a novel two phase hybrid SR generator was introduced, simulated and then fabricated in the laboratory. Some of the generator parameters numerically computed and experimentally measured and tested. The main objectives of this paper, namely introduction of a new two phase field assisted hybrid switched reluctance generator configuration which can produce positive power in all 360° rotor position using the field coil in generating mode as well as producing higher power compare to self excited generator have been achieved. The experimental findings support the simulated results with a difference of less than 20%. The error in generated voltage is caused by considering the field current to be constant in the simulation of the generator unit while in experimental analysis the field current fluctuates due to variable reluctance nature of the generator unit. The experimental analysis shows the functionality of the generator in its new configuration, i.e., it has the ability and the potential of being used in hybrid vehicle or as a generator unit for wind turbine.

ACKNOWLEDGMENT

This work was supported by grant #600/462 from vice-presidency of research and technology of Shahid Beheshti University.

REFERENCES

1. Torrey, D., "Switched reluctance generators and their control," *IEEE Transaction on Industrial Electronic*, Vol. 49, No. 1, 3–14, 2002.
2. Takahashi, A., et al., "Characteristics of 8/6 switched reluctance generator excited by suppression resistor converter," *IEEE Transaction on Magnetics*, Vol. 42, No. 10, 3458–3460, 2006.
3. Mademlis, C. and I. Kioskeridis, "Optimizing performance in current-controlled switched reluctance generators," *IEEE Transaction on Transaction on Energy Conversion*, Vol. 20, No. 3, 556–565, 2005.
4. Chang, Y. and C. Liaw, "On the design of power circuit and control scheme for switched reluctance generator," *IEEE Transaction on Power Electronics*, Vol. 23, No. 1, 445–454, 2008.

5. Radun, A., "Generating with the switched-reluctance motor," *Ninth Annual Applied Power Electronics Conference and Exposition*, 41–47, 1994.
6. MacMinn, S. and J. Sember, "Control of a switched-reluctance aircraft starter-generator over a very wide speed range," *Proc. Intersociety Energy Proceedings of the 24th Intersociety Energy Conversion Engineering Conference*, 631–638, 1989.
7. Ferreira, C., S. Jones, W. Heglund, and W. Jones, "Detailed design of a 30-kW switched reluctance starter/generator system for a gas turbine engine application," *IEEE Transactions on Industry Applications*, Vol. 31, No. 3, 553–561, 1995.
8. Mueller, M., "Design of low speed switched reluctance machines for wind energy converters," *Ninth International Conference on Electrical Machines and Drives*, 60–64, Sep. 1–3, 1999.
9. Cardenas, R., W. Ray, and G. Asher, "Switched reluctance generators for wind energy applications," *26th Annual IEEE Power Electronics Specialists Conference*, Vol. 1, 559–564, 1995.
10. McSwiggan, D., L. Xu, and T. Littler, "Modelling and control of a variable speed switched reluctance generator based wind turbine," *42nd International Universities Power Engineering Conference*, 459–463, 2007.
11. Mueller, M. A., "Design and performance of a 20 kW, 100 rpm, switched reluctance generator for a direct drive wind energy converter," *IEEE International Conference on Electric Machines and Drives*, 56–63, May 15–18, 2005.
12. Martinez, A., et al., "Use of an AC self-excited switched reluctance generator as a battery charger," *13th Power Electronics and Motion Control Conference*, 845–849, Sep. 1–3, 2008.
13. Rabinovici, R. and N. Radimov, "The switched reluctance generator as a flux-compression electromechanical converter," *23rd IEEE Convention of Electrical and Electronics Engineers*, 321–324, Sep. 6–7, 2004.
14. Fahimi, B., A. Emadi, and R. Sepe, "A switched reluctance machine based starter/alternator for more electric cars," *IEEE Transactions on Energy Conversion*, Vol. 19, No. 1, 116–124, 2004.
15. Edrington, C., M. Krishnamurthy, and B. Fahimi, "Bipolar switched reluctance machines: A novel solution for automotive applications," *IEEE Transactions on Vehicular Technology*, Vol. 54, No. 3, 795–808, 2005.
16. Castano, S. and J. Maixc, "Torque control optimization of a switched reluctance motor drive for a 42 V automotive

application," *IEEE International Symposium on Industrial Electronics*, 1171–1176, Jun. 4–7, 2007.

17. Afjei, E., A. Seyadatan, and H. Torkaman, "A new two phase bidirectional hybrid switched reluctance motor/field-assisted generator," *Journal of Applied Sciences*, Vol. 9, No. 4, 765–770, 2009.
18. Afjei, E., O. Hashemipour, and H. Toliyat, "A new hybrid reluctance motor/field-assisted generator," *IEEE International Electric Machines & Drives Conference*, Vol. 1, 543–547, 2007.
19. Qianfan, Z., C. Shumei, and T. Xinjia, "Hybrid switched reluctance motor applied in electric vehicles," *Vehicle Power and Propulsion Conference*, 359–363, Sep. 9–12, 2007.
20. Rahman, K., B. Fahimi, G. Suresh, A. Rajarathnam, and M. Ehsani, "Advantages of switched reluctance motor applications to EV and HEV: Design and control issues," *IEEE Transaction on Industry Applications*, Vol. 36, No. 1, 111–121, 2000.
21. Emadi, A., "Low-voltage switched reluctance machine based traction systems for lightly hybridized vehicles," *Future Transportation Technology Conference & Exposition*, 1–7, 2001.
22. Lehmann, K., G. Probst, and H. Schäfer, "The integrated starter generator as part of the power train management," Aachener Kollequium Fahrzeug-und Motorentechnik, 11, 2000.
23. *MagNet CAD Package: User Manual*, Infolytica Corporation Ltd., Montreal, Canada, 2007.
24. Torkaman, H. and E. Afjei, "Comprehensive study of 2-D and 3-D finite element analysis of a switched reluctance motor," *Journal of Applied Sciences*, Vol. 8, No. 15, 2758–2763, 2008.
25. Torkaman, H. and E. Afjei, "Comprehensive magnetic field-based study on effects of static rotor eccentricity in switched reluctance motor parameters utilizing three-dimensional finite element," *Electromagnetics Journal*, Vol. 29, No. 5, 421–433, Taylor and Francis, 2009.
26. Torkaman, H. and E. Afjei, "Magnetio static field analysis regarding the effects of dynamic eccentricity in switched reluctance motor," *Progress In Electromagnetics Research M*, Vol. 8, 163–180, 2009.